ChemCatChem

Research Article
doi.org/10.1002/cctc.202401338

Chemistry Europe
European Chemical Societies Publishing

www.chemcatchem.org

Multivalent Amine Functionalized Carbon Dots Catalyze Efficient Denitrosylation

Manju Solra,[a] Sourav Das,[a, b] Suman Nayak,[a] Abhay Srivastava,[a] Rohit Kapila,[a] Smarak I. Chaudhury,[a] and Subinoy Rana*[a]

Nitric oxide (NO) is an essential signaling molecule with several biological functions and holds great promise in biomedical applications. However, NO delivery strategies have been challenged with its inherent short half-life and limited transport distance in human tissues. Strategies focused on the catalytic production of NO at the target site would afford an effective biomaterial. Herein, we introduce a carbon dot (CD) platform featuring multivalent amine groups that catalyze the denitrosylation from *S*-nitrosothiols. In the present study, we have developed a novel multivalent amine functionalized carbon dots to catalytically transform endogenous prodrugs *S*-nitrosothiols to generate NO at physiological conditions. The mechanism of NO generation follows a nucleophilic attack of the surface primary amine groups on the electrophilic thiol group of *S*-nitrosothiols, which is supported by various control studies and electron paramagnetic resonance (EPR). Notably, the release of NO is easily tuned by the prodrug concentration and surface density of amines on the CDs. Significantly, the NO-releasing feature of CDs is integrated with the prototissue module to evaluate the NO release profile in the biological environment. This study will deepen our understanding of designing useful multivalent systems to generate NO from endogenous prodrugs to realize their therapeutic potential.

1. Introduction

The discovery of nitric oxide (NO) as a cardiovascular system signaling molecule revolutionized medicine and physiology.[1] The significance of NO in physiological processes has been well understood during late 1980s and early 1990s studies.[2] It was found that NO is a highly reactive molecule with a very short half-life of around 5 s.[3] Despite its transient nature, NO has been shown to play an important role in transmitting cellular signals in mammals,[4,5] due to which it has enormous therapeutic promise, including anticancer therapy,[6] antibacterial/antibiofilm agent,[7] and wound healing.[8] Indeed, several diseases are associated with NO dysregulation, including neurological disorders,[9] inflammatory bowel disease,[10] chronic kidney diseases,[11] retinal ischemia,[12] secondary pulmonary hypertension,[13] and atherosclerosis,[14] which makes a NO delivery at the site of interest an attractive therapeutic avenue.

Nitric oxide delivery technologies face significant limitations due to the physiological properties of NO.[8] In vivo, NO has a very short half-life and can only diffuse over short distances (20–160 μm) because it is rapidly removed by red blood cells and converted to nitrate through its reaction with oxyhemoglobin.[15] To address these challenges, various strategies for effective therapeutic delivery of NO have been developed using endogenous NO donors such as *S*-nitrosothiols (RSNOs).[16] These strategies can be generally categorized into non-catalytic and catalytic approaches. Non-catalytic approaches involve the use of small molecules like ascorbic acid,[17] hydrogen peroxide,[18] sulfur-based nucleophiles (e.g., Na_2SO_3 and Na_2S),[19] and nitrogen nucleophiles (e.g., amines and hydrazine),[20] which can react with and decompose RSNOs via direct nucleophilic attack on the nitroso group. However, the potential cytotoxicity of high concentrations of these compounds, including ascorbic acid, hydrogen peroxide, sulfites, and hydrazine, may limit their biomedical applications. To overcome these limitations, researchers have turned to catalytic approaches, utilizing materials such as gold nanoparticles,[21] copper metal-organic frameworks,[22] and zinc oxide particles[23] to release NO from endogenous prodrugs. Despite their effectiveness, these metal-containing catalysts often require complex synthesis processes and pose potential side effects due to high particle concentrations, which could hinder their practical application. Therefore, there is a need for a metal-free and highly catalytic approach to deliver NO at the target site without causing cytotoxicity.

Carbon dot (CD) is the newest member of the exclusive carbon nano family[24] and has received huge interest due to their controllable photoluminescence, high quantum yield, easily functionalizable, and plentiful low-cost sources.[25,26] Most importantly, notable biocompatibility and low cytotoxicity made the CD a strong competitor to the conventional semiconductor

[a] M. Solra, S. Das, S. Nayak, A. Srivastava, R. Kapila, S. I. Chaudhury, Dr. S. Rana
Materials Research Centre, Indian Institute of Science, C. V. Raman Road, Bangalore 560012, India
E-mail: subinoy@iisc.ac.in

[b] S. Das
Center for Interdisciplinary Research, Institute of Advanced Study in Science and Technology, Paschim Boragaon, Guwahati 781035, India

Supporting information for this article is available on the WWW under https://doi.org/10.1002/10.1002/cctc.202401338

quantum dots in biomedical applications.[27] Tunable electronic properties of CDs allow performance optimization in specific reactions, making them highly versatile in various catalytic applications.[28] The catalytic performance of CDs can be tailored by tuning their sizes, morphologies, and surface properties.[24] The optical properties of the CD cores lead to photocatalysis, which has been applied in organic transformations,[29] as well as in the photodegradation of pollutants,[30] antibiotics and drugs,[30] and in mediating redox biological processes.[31] The high surface area of CDs enables greater interaction with reactants, while the presence of abundant functional groups (hydroxyl, carboxylate, and amine) provides numerous active sites for catalytic reactions, providing efficient synthesis under mild operating conditions.[31] Additionally, the surface functional groups on photoactive CDs have enabled their use in energy-related applications, such as the production of solar fuels via water splitting, and CO_2 reduction processes.[32] Notably, amine-functionalized CDs are known for their distinctive properties and wide-ranging applications in areas like electrocatalysis, targeted drug delivery, and biosensing.[33,34] A primary benefit of these CDs is their improved catalytic performance, as the incorporation of multivalent amine groups amplifies the number of active sites and substrate binding. However, to the best of our knowledge, there are currently no reports on the release of NO from its substrates catalyzed by CDs.

Luo et al.[20] demonstrated that polymeric amine groups can facilitate the release of nitric oxide (NO) from *S*-nitrosothiols. Utilizing the multivalent presentation of amine groups as a covalent catalyst, we explored the catalytic potential of amine-functionalized CDs for NO production. Herein, we synthesized amine-functionalized carbon dots (referred to as BPEI-CDs) and employed them as nucleophilic catalysts to decompose endogenous NO prodrugs for NO release. BPEI, a branched polyethylenimine polymer, contains a high density of nucleophilic primary amine, alongside secondary and tertiary amino groups. This property of BPEI inspired us to utilize it in designing a novel NO-releasing carbon dot (BPEI-CDs) system. In this work, we screened various surface densities of amine-functionalized CDs to assess their effectiveness in generating NO from endogenous prodrugs, demonstrating the crucial role of amines as catalysts. This study provides proof of the concept that amine-functionalized carbon dots can be engineered for controlled and physiologically relevant NO release. We conducted detailed control experiments to investigate the NO release mechanism and assessed the biocompatibility of the synthesized carbon dots. Furthermore, we integrated the new NO release catalyst into a hydrogel-based synthetic prototissue module to verify its biomedical or clinical applicability. The BPEI-CDs showed enhanced NO release in the hydrogel prototissue module, paving the way for new opportunities in NO-generating biomaterials. We envision that the surface engineering of amine-functionalized carbon dots, as developed in this work, establishes a platform for creating advanced NO-release catalysts for therapeutic and biomedical applications.

2. Results and Discussion

2.1. Synthesis of Carbon Dots from Branched Polyethyleneimine (BPEI-CDs)

We synthesized water-soluble BPEI-CDs following a reported protocol[35] via pyrolysis of BPEI at 160 °C. Following the pyrolysis, carbonization of BPEI led to the formation of carbon cores with amines as the surface functional groups (Figure 1a). The as-synthesized BPEI-CDs display a broad absorption band and a strong emission centered at 460 nm upon excitation at 350 nm (Figure 1b). Also, a blue luminescent color was observed under a 370 nm UV lamp (inset of Figure 1b). Moreover, the as-prepared BPEI-CDs exhibit excitation-independent emission spectrum (Figure 1c), unlike most of the reported carbon dots,[8] suggesting a uniform size distribution and homogeneously distributed surface functional groups.[9] The optimal excitation and emission are near 350 and 460 nm, respectively. The average excited state lifetime (τ_{avg}) of BPEI-CDs in the native state was found to be 1.82 ns (Figure S1), which is consistent with the bright blue fluorescent nature of BPEI-CDs.

The uniformity of the BPEI-CD size distribution was observed from high-resolution transmission electron microscopic (HRTEM) images (Figure 1d and S2). As illustrated in Figure 1e, BPEI-CDs displayed an average diameter of ~5 nm with a narrow size distribution of the particles, confirmed through the size distribution of 10 particles in a frame. HRTEM image further highlights the crystalline structure of BPEI-CDs (Figure 1d), with a lattice distance of 0.22 nm, which is consistent with the graphitic (100) lattice plane.[10] These findings suggest that BPEI-CDs contain sp^2 carbon clusters.[10] High-angle annular dark-field (HAADF) imaging was also conducted to visualize the elemental distribution within the BPEI-CDs. In the HAADF images (Figure S2), elemental mapping shows carbon, nitrogen, and oxygen atoms clearly distinguished within the structure, with carbon represented in red, nitrogen in yellow, and oxygen in green. This contrast-enhanced analysis supports the presence of these elements in a homogenous dispersion across the CDs, further validating the composition and uniformity observed in the TEM images. Together, the HRTEM and HAADF analyses provide a comprehensive insight into the structural and compositional characteristics of BPEI-CDs.

In addition, dynamic light scattering (DLS) demonstrated that BPEI-CDs were dispersed uniformly in water with a narrow hydrodynamic diameter distribution (Figure 1f). The powder X-ray diffraction (PXRD) pattern of the BPEI-CDs shows a broad diffraction peak at $2\theta = 21.5°$ (Figure 1g), typical for carbonaceous nanomaterials with highly disordered carbon atoms.[9] The FTIR spectrum of BPEI-CDs (Figure 1h) depicted a broad band with two peaks at 3359 and 3291 cm^{-1} corresponding to the stretching vibration of primary amines, while the bands at 1597 and 1465 cm^{-1} are attributed to the asymmetric and symmetric bending vibration of primary amines (—NH_2).[11] The bands observed at 2941 and 2823 cm^{-1} are attributed to the stretching vibration of —CH_2 group. The significant sharp peaks at 1353 and 1660 cm^{-1} are attributed to the presence of more C—N=

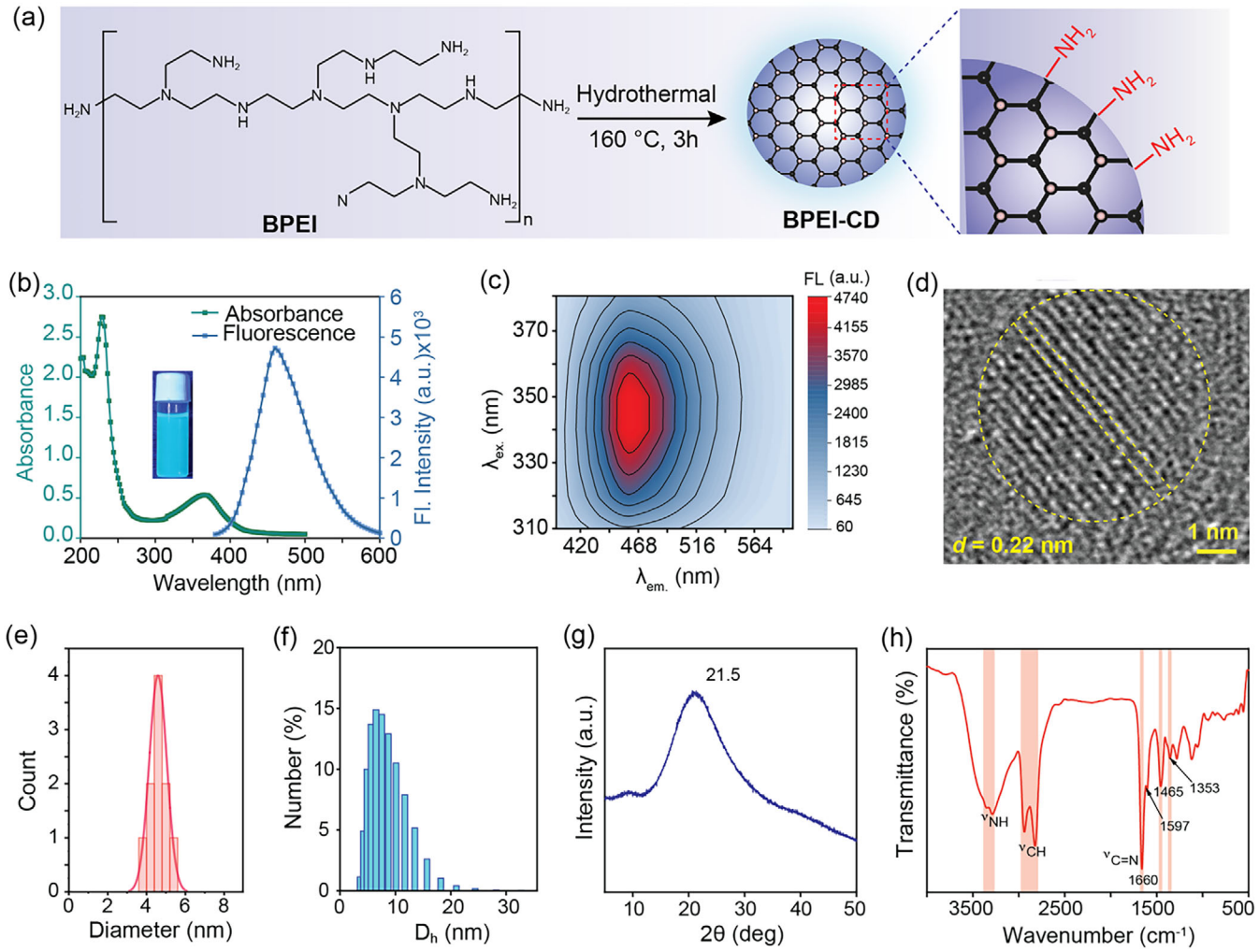

Figure 1. (a) Schematic of the hydrothermally assisted fabrication of BPEI-CDs having a graphitic core with chemically active surface groups. (b) UV–vis absorption and fluorescence emission profiles of the BPEI-CDs. Emission profiles were recorded at λ_{ex} 350 and λ_{em} 460 nm. Here, λ_{ex} and λ_{em} are defined as excitation and emission wavelength, respectively. Inset: Blue fluorescent BPEI-CDs upon irradiation with a UV lamp of 370 nm. (c) A contour plot of BPEI-CDs with varying excitation and emission wavelengths. The fluorescence intensity is abbreviated as FL. (d) HRTEM image of BPEI-CD with lattice planes highlighted by yellow dotted lines. (e) Particle size distribution derived from the HRTEM image, $n = 10$. The diameter of each particle was estimated using Image J software. (f) The hydrodynamic diameter (D_h) of the BPEI-CDs determined through DLS measurements at room temperature. (g) A PXRD profile of the BPEI-CDs showing a peak at 2θ of 21.5°, which is characteristic of the carbonaceous nature of the particles. (h) A FTIR spectrum of BPEI-CDs.

and C═N bonds, thus confirming that these CDs contained an increased amount of graphitic nitrogen.[12] Therefore, the FTIR studies indicate that the surface of the CDs is decorated with primary amines. As the surface of the CDs is functionalized with amines, we tested the influence of pH (1–14) on the fluorescence property of the BPEI-CDs solution. As depicted in Figure S3, the fluorescence intensity of BPEI-CD remained relatively unchanged within pH 1–5 but showed a decreasing trend with an increase in the basicity of the solution. At pH 8, the intensity decreased by ~14%, whereas a further increase in the basicity of the solution led to 35% quenching in the emission intensity of BPEI-CDs at pH 14. In summary, BPEI-CDs are well-dispersed in aqueous solutions, showing a uniform particle size of ~5 nm. The surface of these CDs is decorated with primary amine groups, which contribute to their stability and endow them with efficient catalytic properties.

2.2. Denitrosylation of *S*-Nitrosoglutathione (GSNO)

Following the successful synthesis of BPEI-CDs, we assessed their catalytic ability with GSNO, an endogenously abundant NO donor (Figure 2a). GSNO was synthesized by reacting reduced glutathione (GSH) with hydrochloric acid (HCl) and sodium nitrite ($NaNO_2$). The denitrosylation of GSNO was monitored spectrophotometrically by following the decrease in the absorbance of GSNO at 335 nm over time (in 10 mM HEPES, pH 7.4). As GSNO undergoes denitrosylation, they lose their characteristic absorbance at 335 nm, as shown in Figure S4, indicating that BPEI-CDs are efficient in the denitrosylation of GSNO. In a recent study by Luo et al., it was demonstrated that polymeric amines can induce denitrosylation of *S*-nitrosothiols through nucleophilic reaction of the primary amines with the electrophilic thiol center of nitrosothiol.[20] We hypothesized

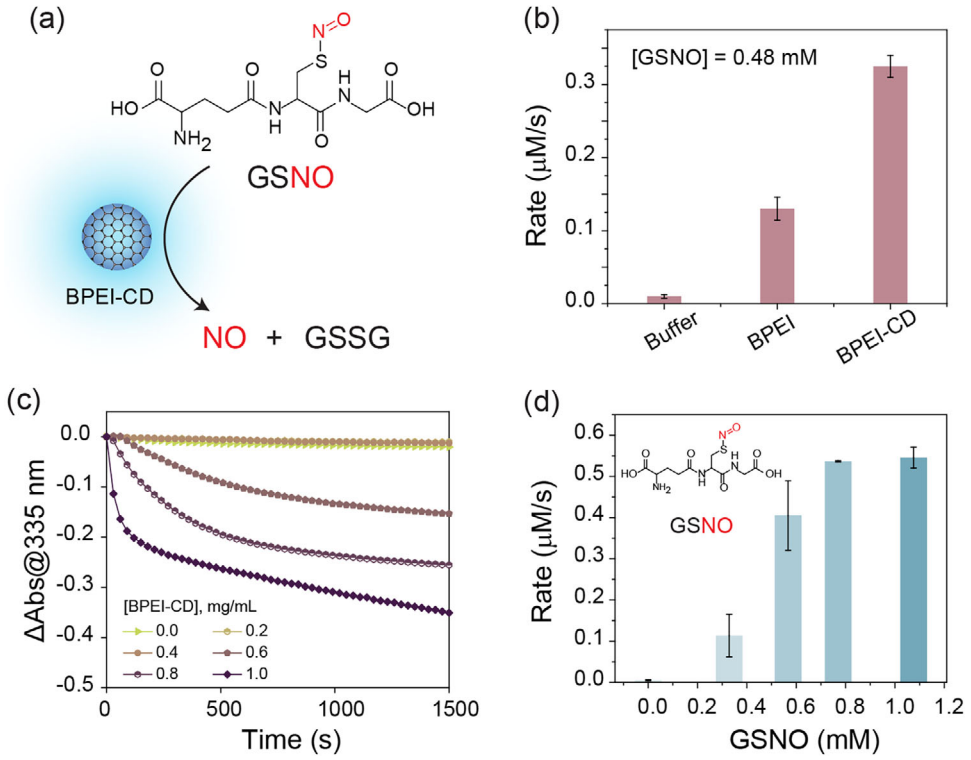

Figure 2. (a) Schematic representation of BPEI-CD as a denitrosylating catalyst. (b) Rate of denitrosylation of BPEI-CD and other relevant controls. [GSNO] = 0.48 mM, [BPEI-CD] = 1 mg/mL, [BPEI] = 1 mg/mL. (c) Kinetic profile of denitrosylation of GSNO at 335 nm in the presence of varying BPEI-CDs concentration over time at 25 °C. [GSNO] = 2.5 mM in 10 mM HEPES pH 7.4. (d) Rate of denitrosylation of varying concentrations of GSNO at 335 nm in the presence of BPEI-CDs (1 mg/mL) at 25 °C in 10 mM HEPES pH 7.4 buffer. The error bars represent the standard deviations of three independent measurements.

that multivalent presentation of primary amine groups on the BPEI-CDs at a higher surface-to-volume ratio would exhibit catalytic denitrosylation from *S*-nitrosothiol prodrugs (Figure 2a). We began investigating the NO-releasing capability using *S*-nitrosylated glutathione (GSNO), as it is one of the most abundant endogenous NO donors present in the blood and tissues.[3] As shown in Figure 2b, BPEI-CDs facilitated NO release from GSNO at a rate of ~threefold higher compared to that achieved with the parent BPEI polymer. This increased rate can be attributed to the higher surface-to-volume ratio of the carbon dots, presenting dense amine groups on the particle surface to facilitate multivalent interaction with the substrate.[36] Subsequently, we studied the catalyst concentration dependence that displayed an enhanced rate of denitrosylation with increasing BPEI-CD concentration, measured by the rapidly declining absorbance at 335 nm with 1 mg/mL of BPEI-CDs (Figure 2c). To demonstrate tunable and controlled NO generation, NO release from GSNO solutions at a wide range of concentrations (0.1–1 mM) was measured in the presence of 1 mg/mL BPEI-CDs. Upon variation of GSNO concentration, a steep decline in the absorbance at 335 nm of GSNO could be observed upon increasing the concentration of GSNO as shown in Figure S5. The rate of denitrosylation determined from the change in absorbance per second showed that the rate increases (Figure 2d) with GSNO concentration, indicating the direct role of BPEI-CDs in the denitrosylation reaction.

To confirm the role of primary amines in denitrosylation, we sought to study the catalytic rate of denitrosylation by various BPEI-CDs with different surface amine densities. Using varied feeding ratios of BPEI and citric acid (CA), we produced different batches of CDs such as CD-75 (75% BPEI, 25% CA), CD-50 (50% BPEI, 50% CA), CD-25 (25% BPEI, 75% CA), and BPEI-CD (100% BPEI, 0% CA) (Figure 3a). Using a ninhydrin assay (see Methods in the Supporting Information), we observed varying primary amine concentrations commensurate with the feeding ratio (Figure 3b). The carbon dot with no amine groups, namely, CD-0 (0% BPEI, 100% CA), provides an important control to illustrate the amine dependency of the catalytic denitrosylation. The prepared carbon dots exhibited an absorption band at 320 nm and an emission maximum at 425 nm (Figure S6), which is quite similar to that of BPEI-CD.

Next, we examined the catalytic activities of these carbon dots using GSNO as a substrate. To further confirm the varying amine densities on the carbon dots, we performed zeta potential and FTIR analyses. As shown in Figure 3c, the zeta potential increases with the feeding ratio of BPEI, indicating a higher concentration of primary amines on the CD surface. Additionally, we observed a gradual decrease in the stretching bands at 3359 and 3291 cm^{-1} (corresponds to N—H), alongside an increase in

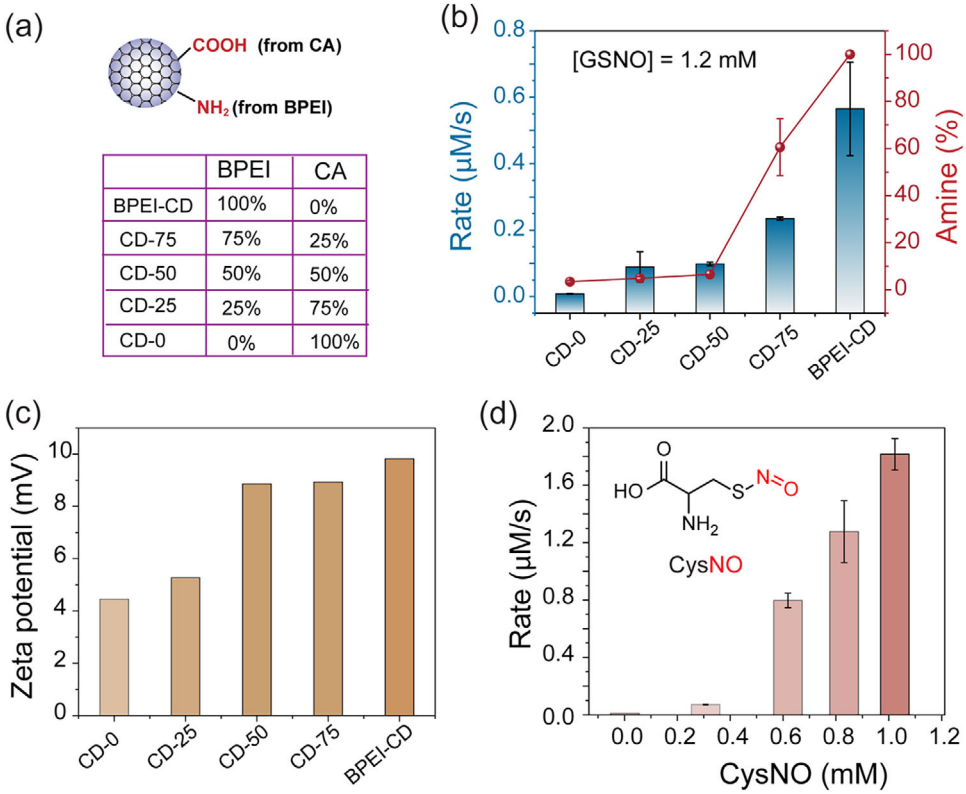

Figure 3. (a) Schematic representation of carbon dots with different densities of amine to carboxylic acid groups. (b) Rate of denitrosylation using carbon dots with different amine densities, keeping the GSNO concentration (1.2 mM) fixed. While the bar plots correspond to the rate, the red dots refer to the amine percentage. The error bars represent the standard deviations of three independent measurements. (c) Zeta potential of the carbon dots with different amine densities. (d) The NO release kinetics of CysNO using BPEI-CD as a catalyst (1 mg/mL). The error bars represent the standard deviations of three independent measurements.

the stretching band at 1703 cm^{-1} (corresponds to C═O), highlighting the varying amounts of primary amines and carboxylic acids on the surfaces (Figure S7). Based on these FTIR and zeta potential results, we hypothesized that BPEI-CDs with the highest amount of surface primary amines would demonstrate the greatest catalytic activity toward GSNO. As shown in Figure 3b, we observed an upregulated rate of denitrosylation by the CDs with a higher percentage of the free primary amine group. For example, BPEI-CD showed a ~sixfold enhanced rate compared to CD-25. Therefore, primary amine density on the CD surface is key to the catalytic activity. Notably, CD-0 without any free primary amine groups failed to produce any denitrosylation activity at the same experiment conditions, elucidating the crucial role of primary amine groups in NO production. To further probe the generalizability of the catalytic efficiency of BPEI-CDs, we tested another nitrosylated endogenous prodrug (CysNO) that contains NO covalently bound to the cysteine thiol. We observed a similar trend with CysNO, showing a substrate concentration-dependent enhancement of the denitrosylation rate (Figure 3d and S8). However, we observed a slightly higher rate of denitrosylation for CysNO compared to GSNO, possibly due to the greater lability of CysNO compared to the glutathione prodrug.[37] This result showed the capability of amine-functionalized carbon dots to decompose GSNO to produce NO and an efficient nucleophilic catalyst.

2.3. Mechanism of Nitric Oxide Release

We continued to probe the NO release mechanism to better understand the role of amine groups on the catalytic denitrosylation. It is well-established that RSNOs possess antagonistic resonance structures, where the sulfur atom can carry either a negative or a positive charge. The presence of a positive charge on the sulfur atom enhances its electrophilicity.[38] Based on the electrophilic character of the thiol group attached to NO, increasing nucleophilicity should drive the denitrosylation reaction forward. To probe the nucleophilicity of the primary amine group, we performed the denitrosylation study at different pHs of 1, 3, 5, and 7.4 (Figure 4a). Notably, the rate of GSNO denitrosylation diminished with the lower pH values, with 60% downregulation of activity at pH 5 while 80% at pH 3 (Figure 4a). This loss of activity is attributed to the protonation of the amine group in acidic conditions. Protonation results in a loss of nucleophilicity of the primary amines, which lowers the nucleophilic attack of amine on GSNO and suppresses the NO release capability. Notably, the BPEI-CDs demonstrated similar catalytic activity both under ambient light conditions and darkness, indicating that the catalytic function is predominantly driven by the presence of primary amine groups rather than any photochemical effects of the CD core (Figure S9). Further, we employed several analytical techniques to understand the nature of intermediates

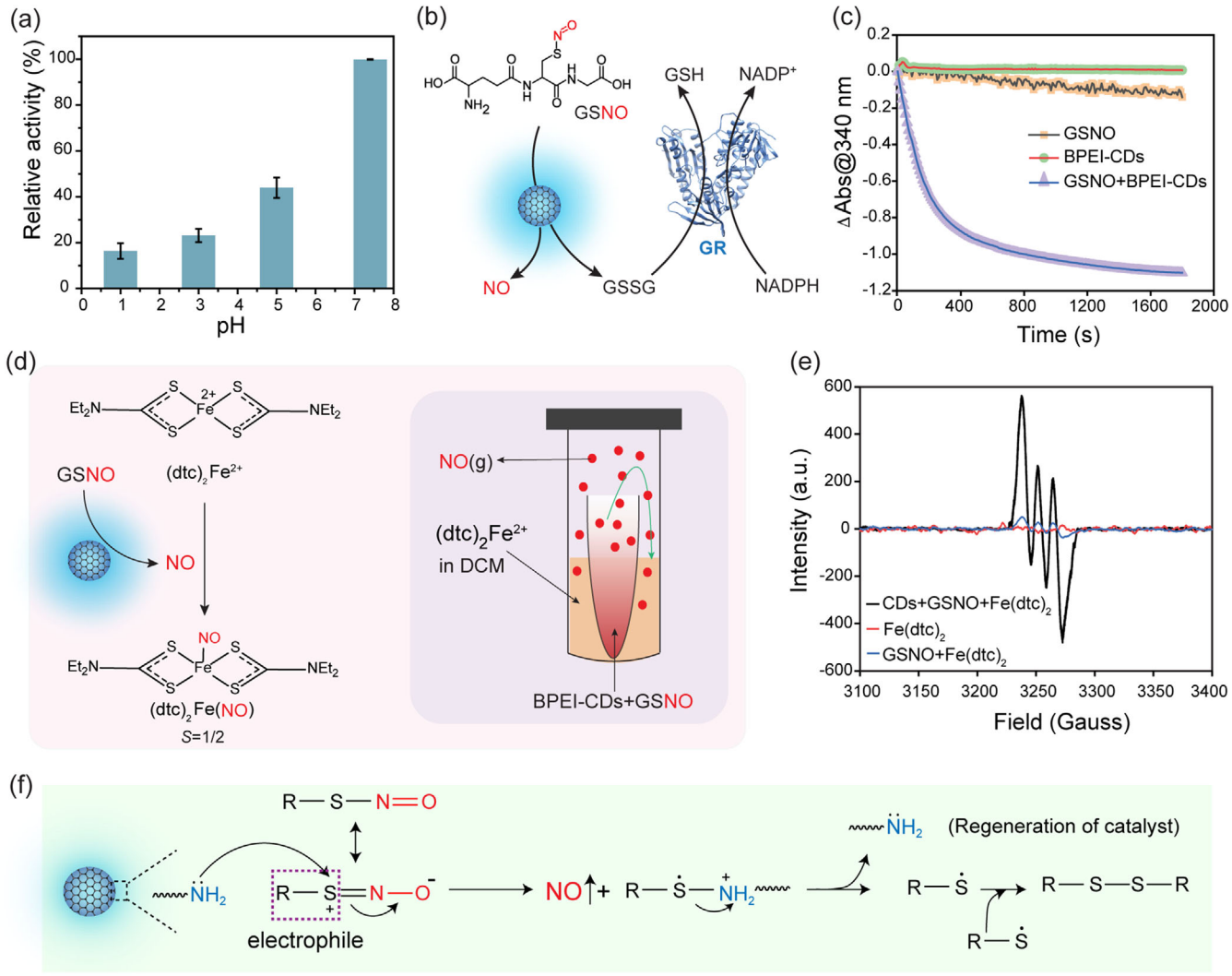

Figure 4. (a) Effect of protonation at denitrosylation activity of BPEI-CDs. [GSNO] = 1.35 mM, [BPEI-CD] = 1 mg/mL. (b) Schematic representation of the coupled assay system involving glutathione reductase (GR) and NADPH to confirm the formation of GSSG. (c) Absorption profile of NADPH at 340 nm upon subjecting to the coupled assay at different conditions at 25 °C. [NADPH] = 0.25 mM, [GR] = 1 U/mL, [GSNO] = 2.5 mM, [BPEI-CDs] = 1 mg/mL, 10 mM HEPES pH 7.4. (d) Schematic showing the reaction of $(dtc)_2Fe^{2+}$ with NO generated from the reaction of GSNO with BPEI-CDs, resulting in the formation of EPR-active $(dtc)_2Fe(NO)$ species. (e) Room temperature EPR spectra of $(dtc)_2Fe^{2+}$ only (red line), $(dtc)_2Fe^{2+}$ with GSNO (blue line), and $(dtc)_2Fe^{2+}$ in the presence of GSNO and BPEI-CDs. (f) Proposed mechanism of NO release from GSNO catalyzed by BPEI-CDs.

formed during catalysis. It has been proposed that denitrosylation of GSNO leads to the generation of glutathione disulfide (GSSG) through the formation of GS• radical intermediate.[39] We verified the formation of the reactive intermediate using a coupled assay in which the formation of GSSG can be confirmed by using the enzyme glutathione reductase (GR) in the presence of a cofactor NADPH (Figure 4b). In mammalian cells, GR catalyzes the reduction of GSSG to its reduced form (GSH) in the presence of NADPH.[40] GSSG reduction can be monitored by measuring the decrease in NADPH absorbance at 340 nm, which corresponds to its reduction to $NADP^+$. The GR activity was evaluated by measuring the decline in the absorbance of NADPH at 340 nm following a 2 h incubation of GSNO with BPEI-CDs. From Figure 4c, the absorption of NADPH showed a rapid decrease, indicating that the reaction of GSNO with BPEI-CDs produces GSSG in addition to NO. The control experiments consisting of only GSNO or BPEI-CDs showed no apparent change in the absorbance kinetics of NADPH when subjected to the GR assay. These results confirm that the BPEI-CDs induce NO release from GSNO while producing GSSG in the system.

Next, we confirmed the BPEI-CDs-mediated release of NO from GSNO using electron paramagnetic resonance (EPR) experiment. For this experiment, we utilized $(dtc)_2Fe^{2+}$ as a NO trapping agent, which gets converted to EPR-active $(dtc)_2Fe(NO)$ as shown in Figure 4d.[41] A vial containing BPEI-CDs (1 mg/mL) and GSNO (20 mM) in 10 mM HEPES pH 7.4 was placed carefully inside a bigger tube containing $(dtc)_2Fe^{2+}$ in dichloromethane. The larger tube was tightly sealed so that the released NO could not escape out (Figure 4e). This ensured that the in situ generated NO diffuses out from the smaller vial and reacts with the $(dtc)_2Fe^{2+}$ generating EPR active $(dtc)_2Fe(NO)$. The room temperature EPR spectrum of this reaction product depicts three distinct splitting patterns ($S = 1/2$) at $g = 2.02$ and $A(^{14}N) = 12.9$ G (Figure 4e), which are characteristic of the $(dtc)_2Fe(NO)$.[41,42] In

sharp contrast, GSNO without BPEI-CDs showed a faint EPR signal, indicating that the uncatalyzed NO release is significantly slow, producing a negligible amount of $(dtc)_2Fe(NO)$ complex under identical experimental conditions. Overall, these results validate the nucleophilic attack of BPEI-CDs surface amine on GSNO and following the release of NO and GSSG (Figure 4f).

To evaluate the selectivity of the catalyst toward RSNO, various control experiments were conducted under the same experimental conditions. Initially, the BPEI-CDs catalyst was tested for its ability to induce nitric oxide from GSNO in the presence of different potential interfering ions. As shown in Figure 5a, BPEI-CDs retained nearly 100% catalytic activity, indicating that the presence of interfering ions did not affect its performance. Subsequently, the selectivity of BPEI-CDs toward GSNO was tested using various molecules, including BSA, HSA, GSH, and $NaNO_2$ (Figure 5b). The results showed that BPEI-CDs exhibited high catalytic activity toward GSNO while showing negligible activity toward the other interferants. These findings collectively demonstrate the high selectivity of BPEI-CDs toward GSNO, making it an efficient catalyst for inducing nitric oxide from RSNO. To assess the catalytic activity of BPEI-CDs in biological samples, we evaluated NO generation from GSNO in human serum. We spiked GSNO into serum in the presence of BPEI-CDs to test the denitrosylation activity of BPEI-CDs in a complex medium. As shown in Figure 5c, the BPEI-CDs maintained their catalytic activity and exhibited a similar performance for GSNO in serum as they did in buffer conditions. Further, a biocompatibility test on a mammalian normal cell line (HEK-293) shows that BPEI-CDs maintain 100% cell viability at lower concentrations (1–25 μg/mL), with moderate toxicity observed at concentrations above 50 μg/mL (Figure S10). These results underscore the potential of BPEI-CDs for biomedical applications, including cancer treatment and wound healing.

2.4. Release of NO Inside a Model Prototissue

Having established the procedure for utilizing BPEI-CDs as a catalyst for generating NO, we aimed to verify the NO release capability of BPEI-CDs in a biological environment by fabricating a model prototissue using agarose gel.[43,44] We designed concentrically arranged hydrogel prototissue modules comprising Griess reagent, BPEI-CDs, and GSNO in the outer, middle, and inner layers, respectively (Figure 6a). Griess reagent is a chromogenic substrate that turns pink on reaction with NO.[45] BPEI-CD reacts with GSNO to produce NO, enabling in situ NO production within the model prototissue to act as a diffusive signal in the central channel of the circular model. To achieve this, we added GSNO to the middle layer of the hydrogel by creating a hole in the module, as illustrated in Figure 6a. Over time, GSNO diffuses into the BPEI-CD layer, facilitating NO formation. The in situ generated NO then reacts with the Griess reagent, forming a pink-colored ring (Figure 6b). In contrast, the

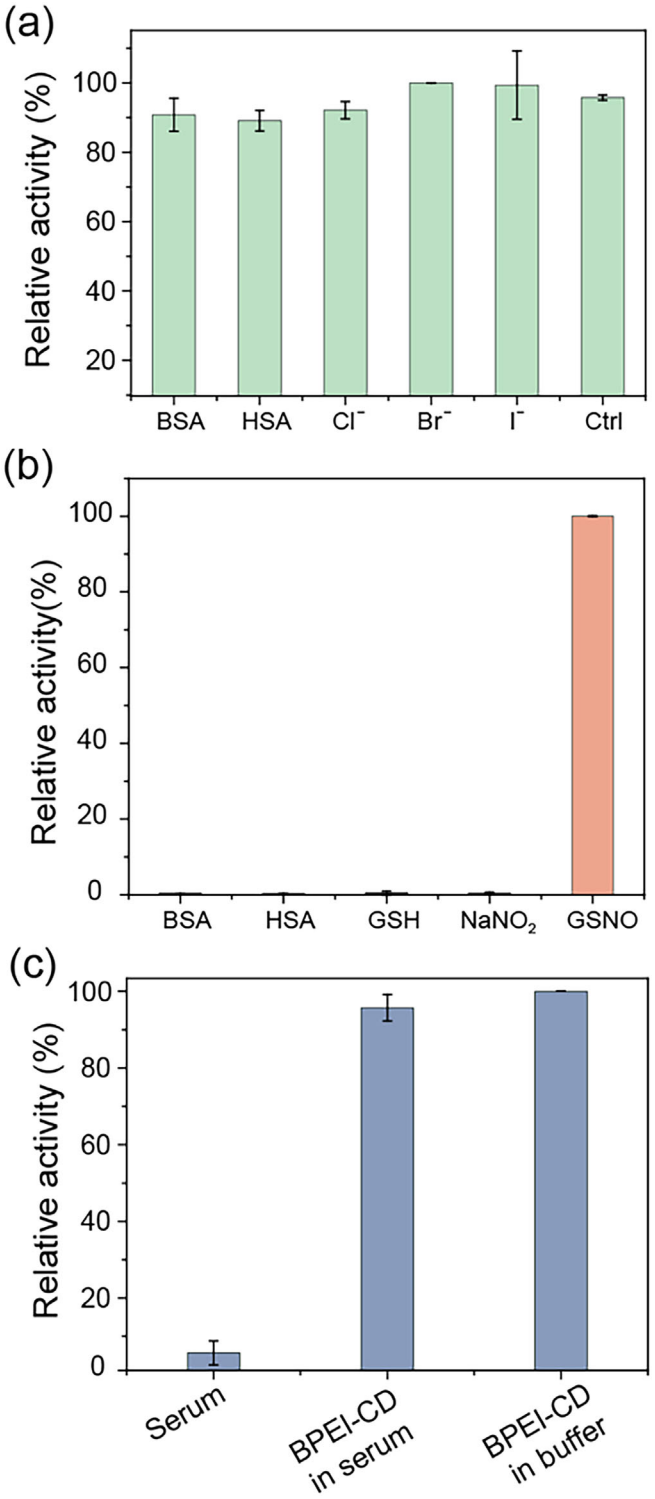

Figure 5. (a) Relative activity of BPEI-CDs in the presence of interfering ions. [Interfering ions] = 1 mM, [BPEI-CDs] = 1 mg/mL, [GSNO] = 1.23 mM. (b) Selectivity of BPEI-CDs toward GSNO in the presence of various potential interferents. The concentration of each analyte was fixed at 1 mM. (c) Catalytic activity of BPEI-CD incubated with GSNO in the human serum. [Serum] = 1%, [BPEI-CDs] = 2 mg/mL and [GSNO] = 2.5 mM.

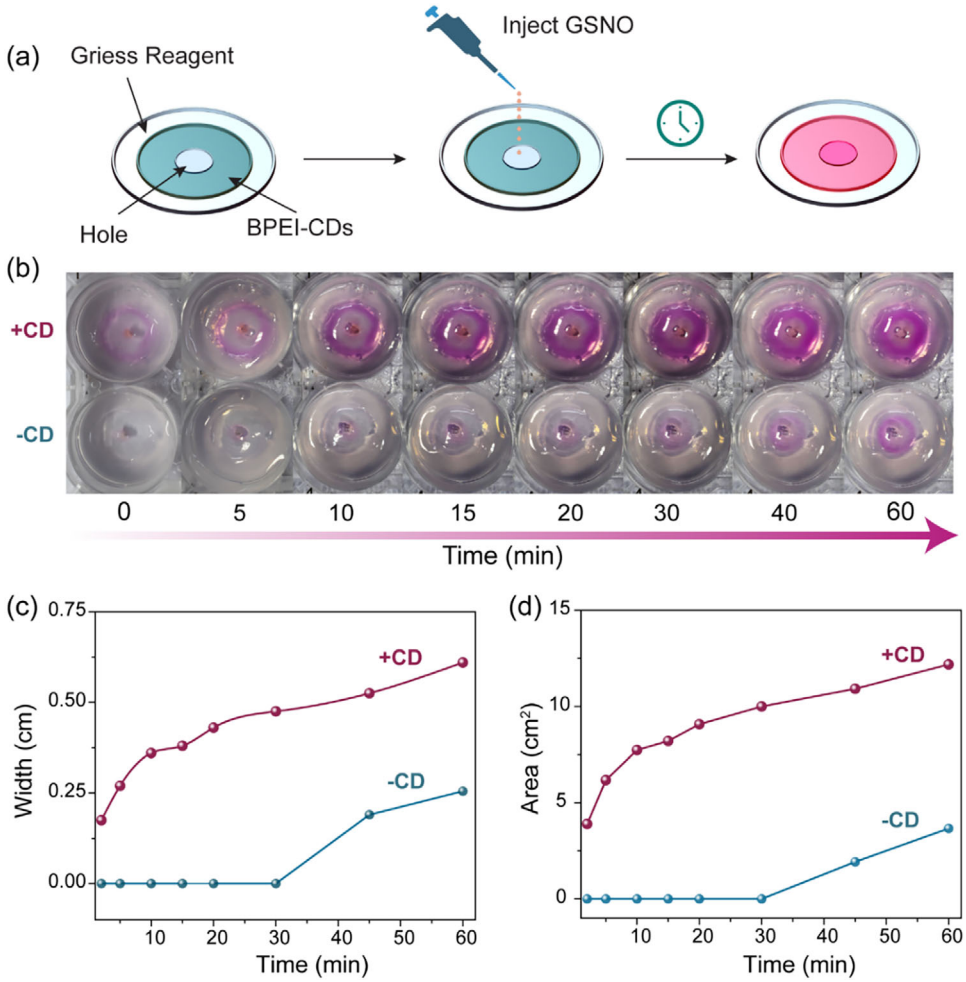

Figure 6. (a) Schematic design for NO release inside agarose hydrogels. The outer ring contains Griess reagent (20 mg/mL), the darker grey circle contains BPEI-CDs, and the central white circle is a hole for injecting GSNO (100 μM) via syringe. For the control study, the hole was filled with Milli-Q water. Injection of GSNO into the hole results in the generation of pink color over time in the middle circle containing BPEI-CDs. (b) NO generation inside the prototissue model with time, probed by the pink-colored compound formation. The top row shows the reaction in the presence of CD (denoted as +CD), and the bottom row contains the control without CD (denoted as −CD). The corresponding (c) width and (d) area of the pink-colored circle formed in the prototissue model.

absence of BPEI-CDs in the middle layer resulted in negligible color formation, underscoring the critical role of BPEI-CDs as a NO release catalyst. To quantify the colored ring formation, we measured the area and width of the pink ring and plotted these against time. The results showed that the area and width of the colored ring increased over time, indicating effective NO release. Notably, the area and width of the colored ring were greater in the presence of BPEI-CDs in the middle hydrogel circle compared to the control prototissue without BPEI-CD (Figures 6c and 6d). This observation was attributed to the catalytic activity of BPEI-CDs in generating NO from GSNO. The NO release displayed sustained release over time, which mimicked the diffusion-limited drug release from a prodrug in the tissue environment. The amount of NO produced was dependent on the quantity of GSNO added to the middle of the prototissue module. Overall, our findings confirm that BPEI-CDs can function as effective denitrosylating catalysts in a biological medium, as demonstrated by the designed prototissue model.

3. Conclusion

In this work, we demonstrated effective denitrosylation of *S*-nitrosothiol prodrugs using multivalent CDs based on BPEI. A straightforward hydrothermal synthesis provided the BPEI-CDs that exhibited desirable properties, including a broad absorption band, bright emission at 460 nm, excitation-independent emission, and uniform particle size. We demonstrated the capability of BPEI-CDs to catalyze the denitrosylation of *S*-nitrosoglutathione (GSNO) and cysteine nitrosothiol (CysNO), leading to effective NO release, catalyzed by the multiple primary amines on the CD surface. Our study revealed that the denitrosylation process was dependent on the concentration of BPEI-CDs and the pH of the solution, with the rate of NO release decreasing in more acidic conditions due to the protonation of the amine groups. Further experiments confirmed the generation of glutathione disulfide (GSSG) as a byproduct of the catalysis. The EPR experiments verified the release of NO from GSNO by trapping the NO with $(dtc)_2Fe^{2+}$, forming an EPR-active

complex. These experiments validate the central role of the multivalent amine groups on the CD surface in the catalytic denitrosylation reaction.

Additionally, we demonstrated the selectivity of BPEI-CDs toward GSNO in the presence of various potential interfering ions and molecules, proving the efficiency and specificity of BPEI-CDs as NO-releasing catalysts. The practical application of these findings was validated by acceptable biocompatibility and integration of BPEI-CDs into a hydrogel-based prototissue module. The in situ generation of NO from GSNO led to observable changes in the prototissue, confirming the biological relevance of our approach. Overall, this study establishes amine-functionalized carbon dots as a robust platform for efficient and selective catalysis to generate NO in biorelevant conditions, paving the way for their application in therapeutic and biomedical fields.[46] The ability to engineer surface properties of carbon dots to control NO release opens new opportunities for developing advanced biomaterials for clinical use.

4. Experimental Section

4.1. Synthesis of BPEI-CD

The synthesis of BPEI-CD was done using the reported protocol.[35] Carbon dots were synthesized using a hydrothermal method, with branched polyethyleneimine (BPEI) serving as the carbon source. Initially, 6.75 g of BPEI was dissolved in 40 mL of Milli-Q water to prepare an aqueous solution. This solution was then transferred into a 50-mL Teflon-lined stainless-steel autoclave and heated at 160 °C for 3 h. After the reaction, a sticky yellow product was obtained from the autoclave, which was then dispersed in ethanol. The resulting ethanolic solution was centrifuged at 10,000 rpm for 10 min using a microcentrifuge. The supernatant, containing the carbon dots (BPEI-CDs), was collected and subsequently characterized.

4.2. Synthesis of Different Carbon Dots

CD-0: An aqueous solution of citric acid was prepared by dissolving 6.75 g of citric acid in 40 mL of Milli-Q water. This solution was then transferred into a 50-mL Teflon-lined stainless-steel autoclave and heated at 160 °C for 3 h. The resulting solution was then subjected to dialysis, followed by concentration using a rotary evaporator.

CD-25: An aqueous solution of citric acid was prepared by dissolving 1.68 g of BPEI and 5.06 g of citric acid in 40 mL of Mili-Q water. This solution was then transferred into a 50-mL Teflon-lined stainless-steel autoclave and heated at 160 °C for 3 h. The resulting solution was then subjected to dialysis, followed by concentration using a rotary evaporator.

CD-50: An aqueous solution of citric acid was prepared by dissolving 3.37 g of BPEI and 3.37 g of citric acid in 40 mL of Mili-Q water. This solution was then transferred into a 50-mL Teflon-lined stainless-steel autoclave and heated at 160 °C for 3 h. The resulting solution was then subjected to dialysis, followed by concentration using a rotary evaporator.

CD-75: An aqueous solution of citric acid was prepared by dissolving 5.06 g of BPEI and 1.68 g of citric acid in 40 mL of Mili-Q water. This solution was then transferred into a 50-mL Teflon-lined stainless-steel autoclave and heated at 160 °C for 3 h. The resulting solution was then subjected to dialysis, followed by concentration using a rotary evaporator.

4.3. Synthesis of RSNO

The synthesis of RSNO was performed using the reported protocol.[42] Glutathione (GSH, 100 mg, 0.325 mmol) was dissolved in 383 µL of ultrapure water and treated with 38 µL of concentrated hydrochloric acid. The solution was stirred in an ice bath (0–4 °C), maintaining the pH between 1 and 2. Once the GSH had completely dissolved, 23 mg (0.325 mmol) of sodium nitrite was added in the dark, causing the solution to turn red immediately. After stirring for an additional 10 min, the red solution was aliquoted into Eppendorf tubes and stored at −20 °C. CysNO was prepared using the same procedure, with cysteine substituted for glutathione.

4.4. Catalytic Activity of BPEI-CD

The catalytic activity of BPEI-CD was monitored using a plate reader. The kinetics were monitored by measuring the decrease in absorbance at 335 nm. The rate of denitrosylation was measured using Equation (1), as follows:

$$\text{Rate} = \frac{\text{Slope}}{\varepsilon l} \qquad ((1))$$

where the slope is defined as the change in absorbance per unit of time, ε (0.92 mM^{-1} cm^{-1} for GSNO, 0.74 mM^{-1} cm^{-1} for CysNO) is denoted as the molar extinction coefficient, and l is referred to as path length (0.58 cm for 200 µL liquid).

4.5. Denitrosylation Using Carbon Dots

Different carbon dots (1 mg/mL) were added to HEPES buffer (10 mM, pH 7.4) in 96-well plates. Subsequently, GSNO was added to the plates, and the kinetics were recorded at absorbance at 335 nm. The rate of denitrosylation was calculated using Equation (1).

4.6. Detection of Nitric Oxide by EPR Spectroscopy

$Fe(dtc)_2$ was used to probe the generated nitric oxide by EPR spectroscopy. An Eppendorf tube (0.5 mL) containing GSNO (1 mM) and BPEI-CD (1 mg/mL) was carefully placed inside a larger Eppendorf tube (5 mL) containing $Fe(dtc)_2$ in dichloromethane, ensuring that the two solutions remained separate. The larger Eppendorf tube was incubated for 45 min, with occasional shaking. After incubation, 50 µL of the solution from the larger Eppendorf tube was transferred to a quartz EPR tube, and X-band EPR spectroscopy was performed at room temperature.

4.7. Cytotoxicity of BPEI-CDs

The cytotoxicity effect of BPEI-CD on the HEK-293 cell line (Human Epidermal Keratinocytes) was assessed using the (3-(4,5-dimethylthiazolyl-2)-2, 5-diphenyltetrazolium bromide) (MTT) assay. HEK-293 cells were seeded at a density of 15,000 cells per well in a 96-well plate to reach the desired confluency. CD samples at varying concentrations (1.5–100 µg/mL) were added in triplicate for reliable readings. The plate was then incubated for 24 h at 37 °C with 5% CO_2. Following the incubation, the media was replaced with fresh media containing MTT solution (2 mg/mL in 5% ethanol) and incubated for an additional 3 h. Afterwards, the media was replaced with 200 µL of dimethyl sulfoxide to dissolve the resulting formazan crystals. Absorbance was then measured at 570 nm, and cell viability was calculated relative to the control group.

Acknowledgements

Manju Solra and Sourav Das contributed equally to this work. This project has received major funding from the Department of Biotechnology (BT/PR49984/MED/32/911/2023) and the Science and Engineering Research Board (CRG/2022/009021). The authors acknowledge MoE-STARS (STARS/APR2019/BS/820/FS) for financial support for access to some of the IISc central facilities. Suman Nayak acknowledges the financial support from the SERB for providing the National Post Doctoral Fellowship (PDF/2023/001158). Manju Solra and Rohit Kapila acknowledge the support from UGC for the doctoral fellowships. Abhay Srivastava thanks the prime minister's research fellowship for the doctoral fellowship. Sourav Das gratefully acknowledges the financial support from the DBT-RA Program in Biotechnology and Life Sciences (DBT-RA/2021/January/NE/231).

Conflict of Interests

The authors declare no conflict of interest.

Data Availability Statement

The data that support the findings of this study are available from the corresponding author upon reasonable request.

Keywords: Carbon dot · Catalysis · Denitrosylation · Multivalent · Nitric oxide

[1] O. Smith, *Nat. Med.* **1998**, *4*, 1215.
[2] S. M. Andrabi, N. S. Sharma, A. Karan, S. M. S. Shahriar, B. Cordon, B. Ma, J. Xie, *Adv. Sci.* **2023**, *10*, 2303259.
[3] M. Kelm, *Biochim. Biophys. Acta.* **1999**, *1411*, 273.
[4] C. Farah, L. Y. M. Michel, J. L. Balligand, *Nat. Rev. Cardiol.* **2018**, *15*, 292.
[5] M. Carlström, *Nat. Rev. Nephrol.* **2021**, *17*, 575.
[6] A. B. Seabra, N. Durán, *J. Mater. Chem.* **2010**, *20*, 1624.
[7] L. Yang, E. S. Feura, M. J. R. Ahonen, M. H. Schoenfisch, *Adv. Healthc. Mater.* **2018**, *7*, 1800155.
[8] A. W. Carpenter, M. H. Schoenfisch, *Chem. Soc. Rev.* **2012**, *41*, 3742.
[9] S. Moncada, J. P. Bolaños, *J. Neurochem.* **2006**, *97*, 1676.
[10] G. Kolios, V. Valatas, S. G. Ward, *Immunology*. **2004**, *113*, 427.
[11] C. Baylis, *Nat. Clin. Pract. Nephrol.* **2006**, *2*, 209.
[12] A. H. Neufeld, S.-i. Kawai, S. Das, S. Vora, E. Gachie, J. R. Connor, P. T. Manning, *Exp. Eye Res.* **2002**, *75*, 521.
[13] C. R. Morris, M. T. Gladwin, G. J. Kato, *Curr. Mol. Med.* **2008**, *8*, 620.
[14] U. Förstermann, N. Xia, H. Li, *Circ. Res.* **2017**, *120*, 713.
[15] C. Helms, D. B. Kim-Shapiro, *Free Radical Biol. Med.* **2013**, *61*, 464.
[16] H. Yu, L. X. Cui, N. Huang, Z. L. Yang, *Med. Gas Res.* **2019**, *9*, 184.
[17] A. P. Munro, D. Lyn H Williams, *J. Chem. Soc., Perkin Trans.* **1999**, *2*, 1989.
[18] S. Thomas, S. Kotamraju, J. Zielonka, D. R. Harder, B. Kalyanaraman, *Free Radical Biol. Med.* **2007**, *42*, 1049.
[19] A. P. Munro, D. L. H. Williams, *J. Chem. Soc., Perkin Trans.* **2000**, *2*, 1794.
[20] Z. Luo, G. Ng, Y. Zhou, C. Boyer, R. Chandrawati, *Small* **2023**, *19*, 2200502.
[21] P. Taladriz-Blanco, V. Pastoriza-Santos, J. Pérez-Juste, P. Hervés, *Langmuir* **2013**, *29*, 8061.
[22] P. Zhang, Y. Li, Y. Tang, H. Shen, J. Li, Z. Yi, Q. Ke, H. Xu, *ACS Appl. Mater. Interfaces.* **2020**, *12*, 18319.
[23] T. Yang, A. S. Fruergaard, A. K. Winther, A. N. Zelikin, R. Chandrawati, *Small* **2020**, *16*, 1906744.
[24] P. Zhu, S. Wang, Y. Zhang, Y. Li, Y. Liu, W. Li, Y. Wang, X. Yan, D. Luo, *ACS Appl. Bio Mater.* **2022**, *5*, 2031.
[25] M. Alafeef, I. Srivastava, T. Aditya, D. Pan, *Small* **2024**, *20*, 2303937.
[26] Y. Wang, A. Hu, *J. Mater. Chem. C.* **2014**, *2*, 6921.
[27] J. Liao, Y. Yao, C. H. Lee, Y. Wu, P. Li, *Pharmaceutics* **2021**, *13*, 1872.
[28] A. Paul, M. Kurian in *Carbon Dots in Analytical Chemistry: Detection and Imaging*, (Eds: S. K. Kailasa, C. M. Hussain), Elsevier, Amsterdam, Netherlands, **2023**, p. 337.
[29] C. Rosso, G. Filippini, M. Prato, *ACS Catal.* **2020**, *10*, 8090.
[30] K. Akbar, E. Moretti, A. Vomiero, *Adv. Opt. Mater.* **2021**, *9*, 2100532.
[31] Q. He, L. Zhang, *J. Mater. Chem. B.* **2023**, *11*, 5071.
[32] Y. Yan, J. Chen, N. Li, J. Tian, K. Li, J. Jiang, J. Liu, Q. Tian, P. Chen, *ACS Nano.* **2018**, *12*, 3523.
[33] R. M. Yadav, Z. Li, T. Zhang, O. Sahin, S. Roy, G. Gao, H. Guo, R. Vajtai, L. Wang, P. M. Ajayan, J. Wu, *Adv. Mater.* **2022**, *34*, 2105690.
[34] S. Liu, N. Zhao, Z. Cheng, H. Liu, *Nanoscale* **2015**, *7*, 6836.
[35] U. Baruah, U. Manna, *Chem. Sci.* **2021**, *12*, 2097.
[36] M. Solra, S. Das, A. Srivastava, B. Sen, S. Rana, *ACS Appl. Mater. Interfaces.* **2022**, *14*, 45096.
[37] J. Gu, R. S. Lewis, *Ann. Biomed. Sci.* **2007**, *35*, 1554.
[38] N. Hendinejad, Q. K. Timerghazin, *Phys. Chem. Chem. Phys.* **2020**, *22*, 6595.
[39] K. A. Broniowska, A. R. Diers, N. Hogg, *Biochim. Biophys. Acta.* **2013**, *1830*, 3173.
[40] N. Couto, J. Wood, J. Barber, *Free Radical Biol. Med.* **2016**, *95*, 27.
[41] N. Hogg, *Free Radical Biol. Med.* **2010**, *49*, 122.
[42] S. Ghosh, P. Roy, S. Prasad, G. Mugesh, *Chem. Sci.* **2019**, *10*, 5308.
[43] S. Liu, Y. Zhang, X. He, M. Li, J. Huang, X. Yang, K. Wang, S. Mann, J. Liu, *Nat. Commun.* **2022**, *13*, 5254.
[44] S. Das, M. Solra, J. Sahoo, A. Srivastava, S. Fathima, M. De, S. Rana, *Chem. Mater.* **2024**, *36*, 759.
[45] M. Solra, S. Das, S. Rana, *Sens. Actuators B: Chem.* **2024**, *406*, 135424.
[46] P. Bhatt, M. Solra, S. I. Chaudhury, S. Rana, *Biosensors* **2023**, *13*, 277.

Manuscript received: July 31, 2024
Revised manuscript received: November 11, 2024
Accepted manuscript online: November 18, 2024
Version of record online: ■■, ■■